引用格式：WANG Qiang, WANG Hao, XIAO Cong, et al. Dual-spectroscopy Gas Detection Technique Based on a Quartz Tuning Fork Detector[J]. Acta Photonica Sinica, 2023, 52(3):0352117
王强,王浩,肖聪,等.基于石英音叉探测器的双光谱气体检测技术[J].光子学报,2023,52(3):0352117

基于石英音叉探测器的双光谱气体检测技术

王强,王浩,肖聪,李劲松
(安徽大学 物理与光电工程学院, 合肥 230601)

摘　要:将波长调制光声光谱和光热光谱有效结合,提出了一种基于石英音叉探测器和光声光谱与光热光谱技术有效融合的双光谱气体检测技术。以大气中水汽为分析对象,利用1 392 nm附近的近红外半导体激光器搭建了一套基于石英音叉探测器的双光谱探测系统,结合波长调制技术中相位依赖特性,利用差分原理实现了波长调制光声光谱和光热光谱信号的有效叠加和增强,与传统探测方案中采用的单一光谱检测方法相比,有效利用了激光功率,实验结果显示,所提出的双光谱探测技术的总体信噪比分别是光声光谱与光热光谱信噪比的1.97和1.24倍,有效提升了系统检测灵敏度。

关键词:光声光谱;光热光谱;石英音叉探测器;双光谱技术;气体探测
中图分类号:O433.4　　**文献标识码**:A　　**doi**:10.3788/gzxb20235203.0352117

0　引言

激光光谱是一种基于光与物质相互作用过程(包括吸收、反射、散射、折射、干涉等)而衍生出来的一种分析技术,依据相互作用过程所满足的物理原理和定律,从而反演出待检测物质的浓度等信息[1]。随着现代激光光源和光电探测器件的不断革新,激光光谱技术亦得到快速的发展。从激光光谱系统三个核心器件(即激光光源、吸收池、光电探测器)及信号增强和噪声抑制方面分析,激光光谱学衍生出一系列高级的激光光谱技术或探测方法[2-3]。例如,针对单通吸收池光程的不足而发展起来的各种长程多次反射型吸收池或高精度光学谐振腔,据此形成的长程吸收池光谱、腔衰荡吸收光谱、腔增强吸收光谱或积分腔吸收光谱[4-5]。为了有效抑制激光光谱系统噪声而建立起来的波长调制或频率调制光谱,以及双频调制光谱[6-7]。针对各种光电探测器波长响应带宽有限,以及光信号易产生干涉效应的影响,通过检测声信号,代替传统的光信号检测方式,而衍生出的光声光谱。然而,光声光谱发展的过程中,鉴于传统声信号探测器(如:麦克风)频率响应带宽有限,进一步发展起来了石英音叉光声/光热光谱和微悬臂梁增强光声光谱等[8-15]。这些新型的激光光谱技术具有高灵敏度、高分辨率、快速响应特性和非破坏性等显著优势,在大气环境监测、工业生产控制、生物医学和海洋科学等领域得到广泛的应用[16-18]。

针对传统半导体光电探测器波长或频率响应带宽有限,而无法满足超连续光谱范围及整个电磁波范围内的全波段响应的需求,本课题组以石英音叉为核心器件,利用其压电效应和谐振特性研制了一种成本低廉、波长响应带宽宽广的新型光电探测器[19],多年来,通过将其结合光声光谱、直接吸收光谱、波长调制光谱等光谱分析技术实现了大气温室气体和痕量气体、挥发性有机物等众多气体成分的高灵敏度分析[19-22]。为了进一步提高基于石英音叉激光光谱检测技术的灵敏度,本文开展了一种光声光谱和光热光谱融合的双光谱探测技术,为了检验该探测技术的可靠性,以水汽为分析对象,利用近红外半导体激光器搭建了基于石英音叉探测器的双光谱融合探测系统,并在数据处理方法和系统灵敏度等方面进行了深入研究和性能评估。

基金项目:国家自然科学基金(Nos.41875158, 61675005)
第一作者:王强,b20301093@stu.ahu.edu.cn
通讯作者:李劲松,ljs0625@126.com
收稿日期:2022-09-24;**录用日期**:2022-10-26

1 激光光谱理论

1.1 激光吸收光谱理论

理论上当一束光穿过吸收介质时，入射光强$I(\nu)$与出射光强$I_0(\nu)$之间的关系满足朗伯-比尔定律，其数学表达式为

$$I(\nu)=I_0(\nu)\exp\left[-\alpha(v)CL\right]=I_0\exp\left[-S(T)g(v)PCL\right] \tag{1}$$

式中，$\alpha(v)$表示气体吸收系数，$S(T)$表示气体吸收线强，$g(v)$是吸收系数的线型函数，PCL分别表示气体压强，待测气体浓度和有效光程。本文采用洛伦兹线性函数，在全频域内积分为1，因此可得气体的浓度为

$$C=\frac{\int_{-\infty}^{\infty}-\ln\left(\frac{I(v)}{I_0(v)}\right)\mathrm{d}v}{S(T)PL} \tag{2}$$

采用波长调制光谱可以有效降低低频噪声对探测灵敏度的影响，将高频正弦波叠加在低频三角波信号上，使气体吸收的信息转移到高频段。当气体吸收为弱吸收且在近红外波段目标分子吸收量远小于0.05时，式(1)可以简化为

$$I_v=I_0\exp\left[-\alpha(v)CL\right]=I_0\left[1-PCLS(T)g(v)\right] \tag{3}$$

典型的分子吸收线型包括高斯线型、洛伦兹线型、沃伊特线型，在常压下满足洛伦兹线型，该条件下分子吸收系数的表达式为

$$\alpha(v)=\frac{\alpha_0}{1+\left[\frac{(v-v_0)}{\gamma}\right]^2} \tag{4}$$

式中，α_0是吸收线中心频率的吸收系数，v_0是吸收线的中心频率，γ是吸收线的线宽。当激光器被调制频率为ω的正弦调制信号注入时，其瞬时频率描述为

$$v(t)=\bar{v}+\Delta v\cos(\omega t) \tag{5}$$

式中，$\bar{v}$是激光波长的中心频率，Δv是调制深度。激光强度受电流调制影响，其表示为

$$I_0(t)=\bar{I}\left[1+i_0\cos\left(\omega t+\phi_0\right)\right] \tag{6}$$

在式(6)中，$\bar{I}$是激光在调制中心频率$\bar{v}$的平均强度，$\bar{i}_0$是归一化线性强度调制幅度，ϕ_0是线性强度调制相移。由于非线性调制的幅度很小，所以只考虑线性调制。可以将激光的瞬时输出频率代入吸收系数$\alpha(v)$，并将其展开为傅里叶级数

$$\alpha(v)=\alpha(v+\Delta v\cos(\omega t)) \tag{7}$$

$$\alpha(\bar{v}+\Delta v\cos(\omega t))CL=\sum_{n=0}^{\infty}H_n(\bar{v},\Delta v)\cos(n\omega t) \tag{8}$$

在式(8)中，$H_n(\bar{v},\Delta v)$是吸收系数的傅里叶级数展开系数，对于低浓度的微量气体，n次谐波分量可描述为

$$\begin{cases}H_0(\bar{v},\Delta v)=\dfrac{\alpha_0 CL}{2\pi}\displaystyle\int_{-\pi}^{\pi}\frac{1}{1+\left[(\bar{v}+\Delta v\cos\omega t-v_0)/\gamma\right]^2}\mathrm{d}(\omega t)\\ H_n(\bar{v},\Delta v)=\dfrac{\alpha_0 CL}{\pi}\displaystyle\int_{-\pi}^{\pi}\frac{\cos(n\omega t)}{1+\left[(\bar{v}+\Delta v\cos\omega t-v_0)/\gamma\right]^2}\mathrm{d}(\omega t)\end{cases} \tag{9}$$

由式(9)能够看出，吸收系数傅立叶系数与气体浓度和光程的乘积成正比。在吸收光谱中心频率处，奇次谐波的展开系数为0，偶次谐波的展开系数随阶次的增加而减小。因而，$2f$信号通常被用于气体浓度探测以获得最高的检测灵敏度。

1.2 石英音叉增强型光声/光热光谱

石英音叉增强型光声光谱于2002年被提出，属于光声光谱范畴，通过利用石英音叉的共振效应与压电效应将其作为声信号探测器，将光与气体相互作用后以无辐射弛豫过程释放的声信号转换为电信号。基于石英音叉的光声信号可以表示为

$$S_1 \propto \frac{QP\alpha}{f_0} \tag{10}$$

式中，Q表示音叉的品质因数，P表示激光光功率，α表示分子吸收系数。f_0是石英音叉的中心共振频率。石英音叉的谐振频率可以表示为

$$f=\frac{1}{2\pi}\sqrt{\frac{k}{m_{\text{eff}}}}=1.015\frac{w}{2\pi l^2}\sqrt{\frac{E}{\rho}} \tag{11}$$

式中，$m_{\text{eff}}=0.2427\cdot\rho\cdot l\cdot w\cdot t$为有效质量，$\rho$、$l$、$w$、$t$分别为音叉叉臂的密度、长度、宽度和厚度。$k=\dfrac{1}{4Ew(\dfrac{t}{l})^3}$是弹性常数，$E$是石英的杨氏模量。$Q$反映了石英音叉振动受到的阻尼量，$Q$的计算公式为

$$Q=\frac{f_0}{\Delta f} \tag{12}$$

Δf表示带宽，一般仅有几Hz，f_0表示音叉中心共振频率。

鉴于石英音叉的高品质电子学属性和低廉的价格优势，近年来，石英音叉被广泛用于替代传统的半导体探测器用于光信号探测，进而提出一种基于石英音叉光致热弹性效应的石英增强光热光谱，与上述石英增强光声光谱不同，入射激光直接照射到音叉臂上，当激光被调制且调制频率与其本征频率一致时，石英音叉在辐射力与光热驱动力作用下迫使音叉产生机械共振，最后通过其自身具有的压电效应将光-热信号转为电信号。本质上，石英增强光热光谱亦是一种以石英音叉作为光电信号探测器的光谱技术，原理上与直接吸收光谱或波长调制光谱相似，满足朗伯-比尔定律。

2 石英音叉双光谱技术实验系统

鉴于石英音叉即可作为声信号探测器，又可以作为光信号探测器，本文利用2个石英音叉探测器（QCTF1和QCTF2）同时用于光声信号和光热信号探测，实现一种基于石英音叉的双光谱探测技术。以大气中水汽为研究对象，所搭建的双光谱融合气体探测系统实验装置示意图如图1所示。激光光源为中心波长在1 392.67 nm附近的近红外半导体DFB激光器，激光器波长输出由自主开发的驱动板控制，波长调谐和调制过程分别由信号函数发生器（Tektronix，AFG1022）输出的三角波和锁相放大器（Stanford Research Systems，SR830）输出的正弦波实现，两路电压信号叠加后由驱动板转化成电流信号再输入到激光器，激光器默认温度设置为34℃，使激光器输出激光的波长可有效覆盖H_2O在光波长为1 391.67 nm附近的吸收线。为了便于光路调节，将DFB激光器的出射光直接耦合进入光纤准直器，再通过调整准直器的位置让激光光束穿过QCTF1探测器的两振动臂之间，用于探测激光与水汽吸收过程产生的光声信号，其中准直器的出光

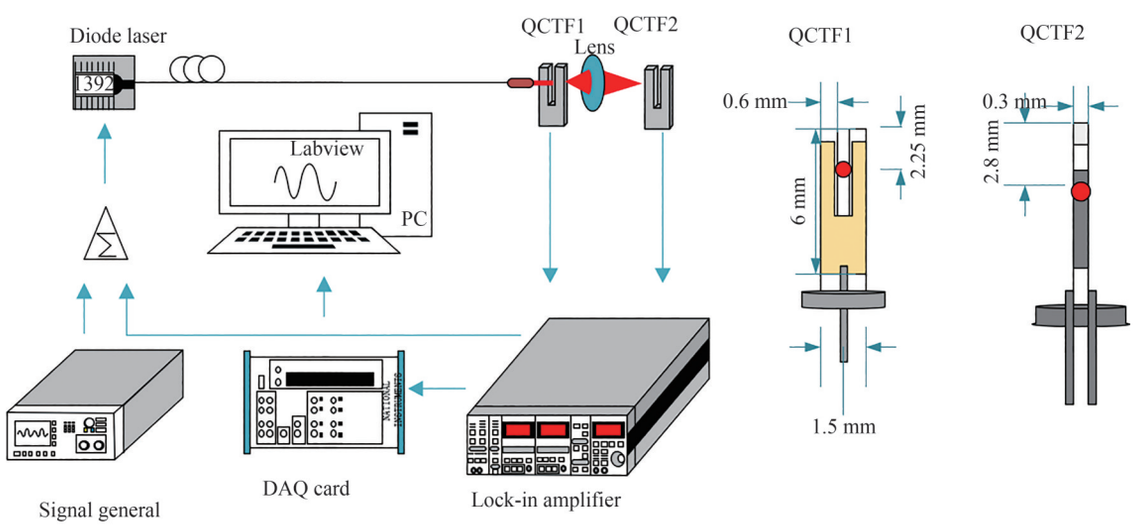

图1 双光谱气体探测技术实验系统示意图

Fig. 1 Schematic diagram of experimental system based on dual-spectroscopy gas detection technique

口与QCTF1的距离为15 cm。透过QCTF1两臂之间的激光光束再通过焦距为5 cm的CaF_2透镜聚焦到QCTF2探测器侧臂表面，用于探测激光与水汽吸收过程产生的光热信号。两路信号同时输入到锁相放大器进行光声光谱信号与光热信号差分解调，解调的信号由数据采集卡(NI USB-6259, 1.25 MHz sampling rate)采集到PC端，最后由自主开发的基于LabVIEW程序的软件进行信号分析与处理。

水汽是一种重要的大气分子，它在空气中含量虽少但却是空气的重要组成部分。为此，本实验选择水汽作为探测的目标气体，以检验所提出的双光谱气体探测技术。基于HITRAN online数据库，首先模拟了H_2O分子在红外区域吸收光谱分布以及空气中的主要干扰气体，如CH_4、CO、CO_2和O_2，模拟结果如图2(a)所示，由此可见H_2O分子在1.39 μm和1.88 μm附近具有相对较强的吸收，图2(b)表示的区域是实验中使用的激光器可实现的波长调谐范围，由此可见，在1 391.67 nm附近，其他气体分子基本没有吸收，可以有效降低干扰气体吸收光谱的影响。表1给出了激光器调谐波长范围内1 391.67 nm附近H_2O分子的吸收谱线参数。由此表可见H_2O在1 391.67 nm附近包括两条吸收线，即使在多普勒加宽条件下亦无法分开，因而有效线强可以看作是两条独立线强的叠加。

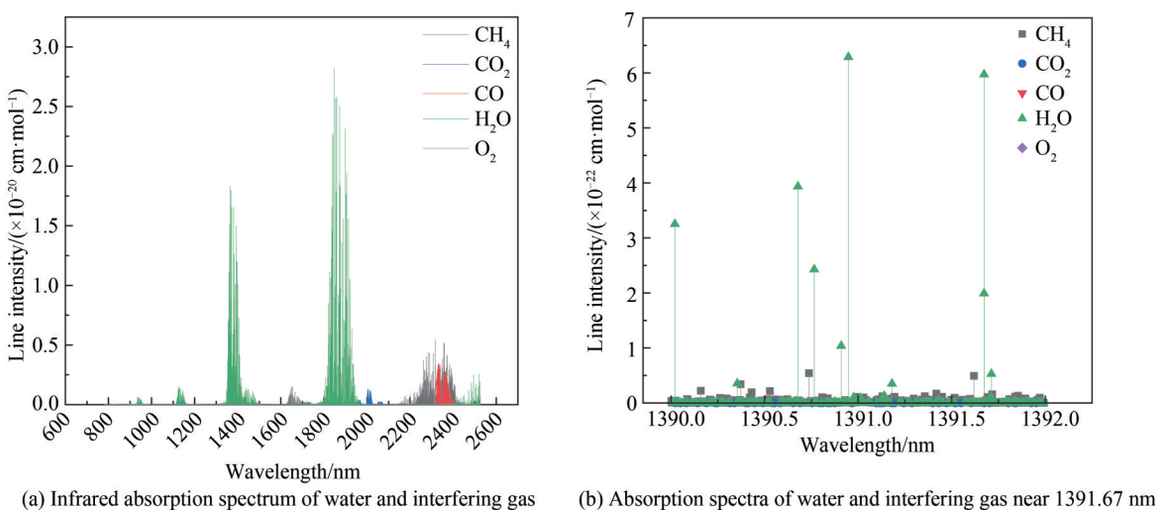

(a) Infrared absorption spectrum of water and interfering gas　(b) Absorption spectra of water and interfering gas near 1391.67 nm

图2　CH_4、CO、CO_2、H_2O、O_2的红外吸收谱线

Fig. 2　Infrared absorption lines of CH_4, CO, CO_2, H_2O, O_2

表1　目标谱线的光谱参数

Table 1　Parameters of spectral line

Species	Wavelength /nm	Wavenumber /cm^{-1}	Line intensity /($cm \cdot mol^{-1}$)
H_2O	1 391.672 99	7 185.596 11	5.971×10^{-22}
H_2O	1 391.672 92	7 185.596 43	1.99×10^{-22}

实验前，首先对激光器的波长调谐特性进行了测量，DFB激光器可以通过改变其输入电流(或电压)和温度来实现不同波长输出。为了精准的控制激光器的输出波长，首先测试了中心波长在1 391.67 nm附近的DFB激光器在工作温度为34 ℃时的电压与波长之间的关系。对于该实验使用高精度波长计(High Finesse Gmbh, WS6-200)记录的工作温度为34 ℃时驱动电压与绝对波长之间的关系如图3所示。根据校正结果，选择激光器的温度为34 ℃，可有效覆盖H_2O在光波长为1 391.67 nm附近的吸收线，该条件下激光器的最大输出功率约为33 mW。

石英音叉作为探测器主要依靠于其共振效应与压电效应，因此为了准确的获取石英音叉的谐振频率特性，在一个大气压下记录了其频率响应曲线如图4所示，同时给出了基于洛伦兹函数的理论计算曲线。由图4可知，QCTF1最佳中心频率f_0=32 760.363 Hz，QCTF2最佳中心频率f_0=32 760.074 Hz，依据品质因子Q值定义：中心谐振频率f_0与信号带宽Δf的比值，计算出所采用2个音叉探测器的品质因数Q值分别为6 891.115和6 355.009，该比值表示信号增强因子。鉴于锁相放大器只能解调一种频率且调制频率越接近中

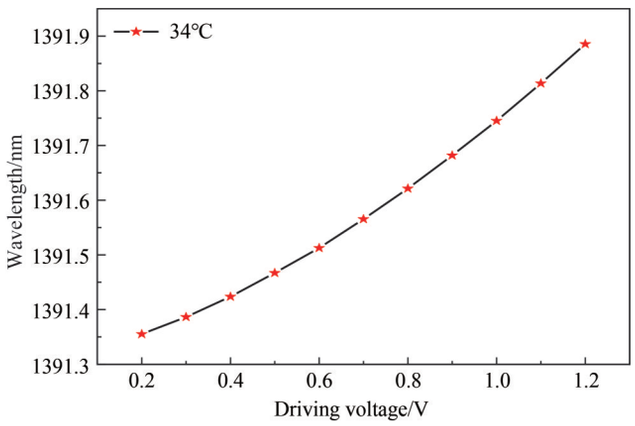

图3　激光器的发射波长与驱动电压的依赖关系

Fig. 3　Relationship between laser emission wavelength and driving voltage

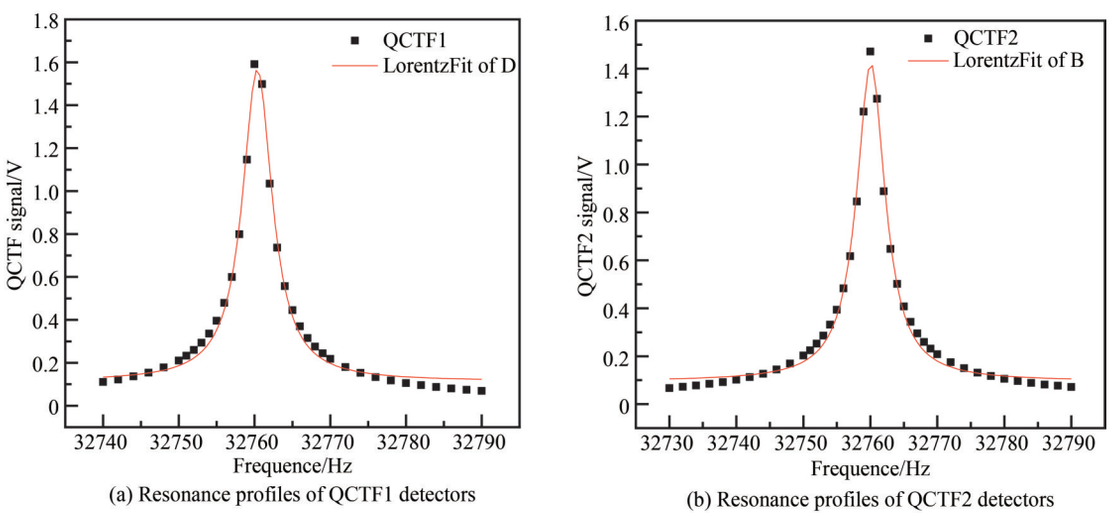

图4　QCTF1和QCTF2石英音叉探测器共振轮廓曲线

Fig. 4　Resonance profiles of QCTF1 and QCTF2 detectors

心频率f_0，音叉共振效果越好，即共振信号越强的原则，最后选定锁相放大器输出的正弦信号频率为32 760 Hz用于调制DFB半导体激光器。

3　实验结果与讨论

基于石英音叉的光声光谱与光热光谱信号幅值与激发位置具有显著的依赖关心，在实验之前，对QCTF1和QCTF2石英音叉探测器的激发位置的进行了优化研究，以获得音叉的最佳激发位置，实验结果如图5所示。图5中纵坐标表示为音叉信号解调后二次谐波的幅值，图5(a)和(b)对应于音叉光声信号与移动距离的关系，由图5中QCTF1左端上顶点为原点，向右为x轴方向，向下为y轴方向移动，可以看出QCTF1音叉探测器在横向0.625 mm，纵向2.25 mm处为最佳激发位置。图5(c)对应于音叉光热信号与移动距离的关系，在图5中QCTF2所表示的音叉上采取激光照射音叉右臂侧面的激发方式，以右臂上顶点中心处为原点，向下为y轴正方向，由图5(c)可得在音叉右臂顶点往下2.8 mm处光热信号最好。

由于波长调制光谱技术中调制相位对调制光谱信号的幅值会造成影响，本实验研究了调制相位对双光谱叠加信号的影响。双光谱融合策略的关键在于两光谱信号相位相反的差分叠加，所以寻找最佳调制相位对于叠加信号的幅值提升具有重要意义。相位调制实验结果如图6所示。图6中横坐标表示调制信号的相位，纵坐标表示QCTF1和QCTF2差分叠加后获得的双光谱信号的幅值。Signal1与Signal2表示相同条件下的相位调制实验两次测量结果，以验证相位调制对音叉信号的影响具有一致可重复性。由图可得相位在70°与－115°时双光谱信号效果最佳。

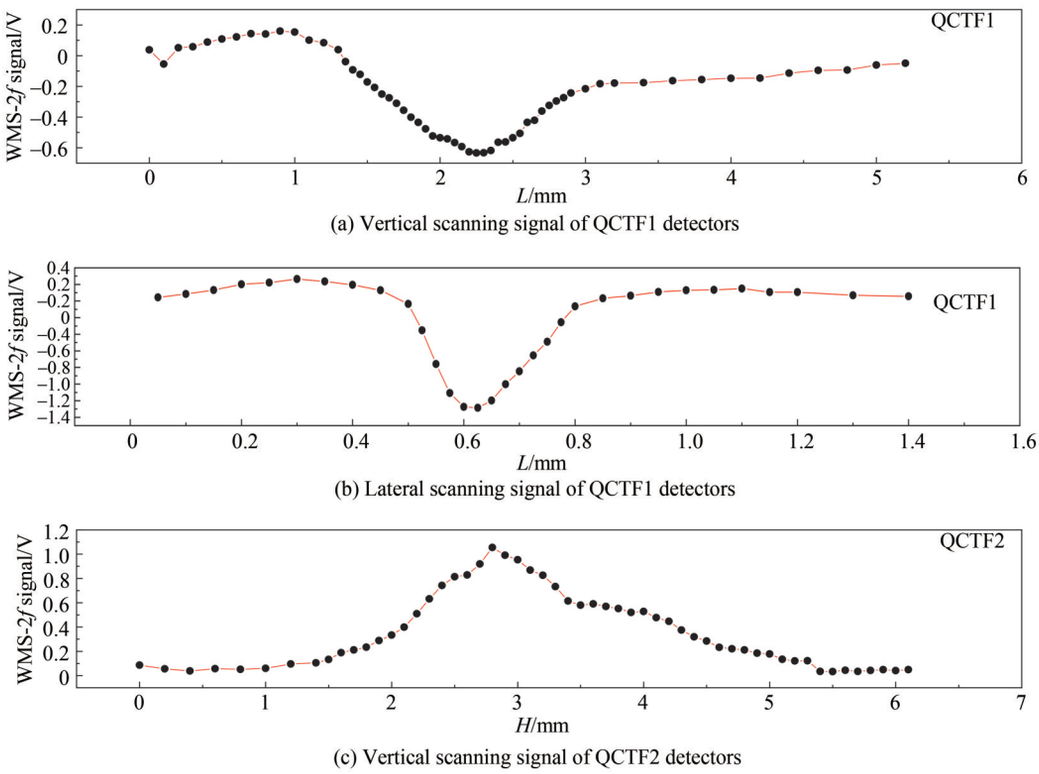

图 5 QCTF 信号幅值与激发位置的函数关系

Fig. 5 Functional relationship between QCTF signal amplitude and excitation position

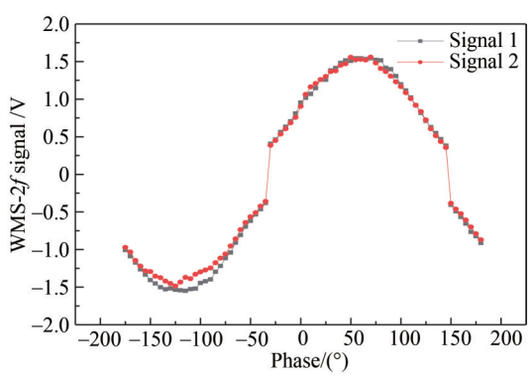

图 6 调制信号相位与双光谱信号幅值的函数关系

Fig. 6 Functional relationship between modulated signal phase and bispectral signal amplitude

在最优激发位置下，采用调制电压相位为 70°，电压为 0.04 mV，频率为 32 760 Hz，测得的 QCTF1 光声信号、QCTF2 光热信号与双光谱信号（QCTF2-QCTF1）如图 7 所示。由图 7 可得，双光谱信号的幅值明显增大，且差分过程亦能明显降低噪声幅值，从而实现光谱信噪比的有效提高，相比于单一光热光谱和光声光谱测量结果，光谱信噪比分别提高了 1.97 和 1.24 倍。

此外，QCTF 的光电转换效率显著依赖于入射激光功率。因此，本文研究了 QCTF 对 DFB 半导体激光器发射功率的响应特性。实验中通过使用光纤衰减器逐步改变入射光强，图 8 给出了输出激光功率与 WMS-2f 信号幅度之间的关系。结果表明，QCTF 探测器对入射激光功率具有良好的线性响应，线性度 R^2=0.996，信号幅值与光功率的关系可表示为 y=−0.061 38+0.047 52x。

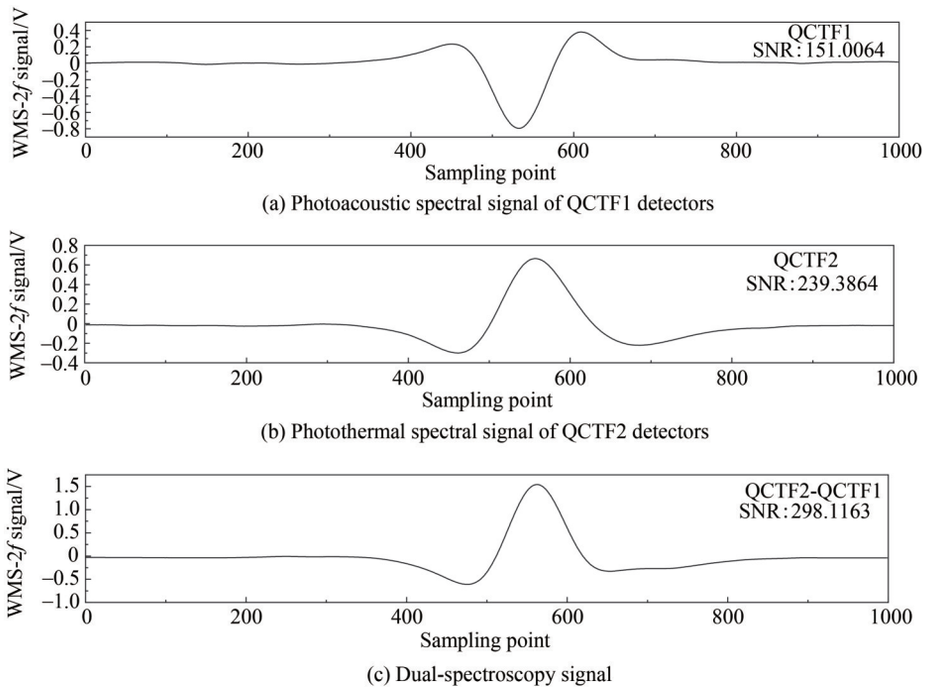

图7　最优条件下测量的H_2O光声光谱、光热光谱与双光谱信号

Fig. 7　Photoacoustic, photothermal and dual-spectroscopy signals under optimal conditions

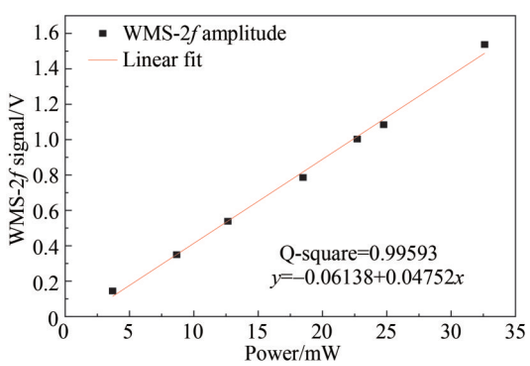

图8　WMS-2F信号幅度随激光功率的变化

Fig. 8　Variation of WMS-2F signal amplitude with laser power

4　结论

石英音叉探测器在光声光谱和光热光谱方面的广泛应用，提出了一种基于石英音叉探测器的光声光谱与光热光谱技术有效融合的双光谱气体检测技术。利用1 392 nm附近的近红外半导体激光器搭建了一套基于石英音叉探测器的双光谱探测系统，结合波长调制技术中相位依赖特性，利用差分原理实现了波长调制光声光谱和光热光谱信号的有效叠加和增强，与传统探测方案中采用单一光谱检测方法相比，有效利用了激光功率。以大气中水汽为分析对象，开展了水汽的实时测量研究。研究表明在调制幅值为0.04 mV，调制相位为70°时，所提出的双光谱探测技术的总体信噪比分别是光声光谱与光热光谱信噪比的1.97和1.24倍，光谱信号信噪比得到了明显提高，有效提升了系统检测灵敏度。

参考文献

[1]　INMAN R S, MCANDREW J. Application of tunable diode laser absorption spectroscopy to trace moisture measurements in gases[J]. Analytical Chemistry, 1994, 66(15): 2471-2479.

[2]　ZHOU Lianjun, HAN Fuzhong, BAI Peiji, et al. Review of HOT MW infrared detector using mct technology[J]. Infrared Technology, 2017, 39(2): 116-124.
周连军，韩福忠，白丕绩，等. 高温碲镉汞中波红外探测器的国内外进展[J]. 红外技术，2017，39(2)：116-124.

[3] HE Wen, WANG Cong, TIAN Zhen, et al. Research on performance regulation technology of Hg Cd Te infrared detector [J]. Infrared, 2021, 42(12): 6-14.
何温, 王丛, 田震, 等. 碲镉汞红外探测器性能调控技术研究[J]. 红外, 2021, 42(12): 6-14.
[4] XU Liuyang, YU Jing, MO Zeqiang, et al. Advances in cavity ring-down absorption spectroscopy research and typical applications[J]. Laser & Optoelectronics Progress, 2021, 58(19): 1-16.
徐毓阳, 余锦, 貊泽强, 等. 腔衰荡吸收光谱技术的研究进展及典型应用. 激光与光电子学进展, 2021, 58(19): 1-16.
[5] CHEN Dongyang, ZHOU Li, YANG Fumo, et al. Application progress of Cavity-Enhanced Absorption Spectroscopy (CEAS) in atmospheric environment research [J]. Spectroscopy and Spectral Analysis, 2021, 41(9): 2688-2695.
陈东阳, 周力, 杨复沫, 等. 腔增强吸收光谱技术在大气环境研究中的应用进展[J]. 光谱学与光谱分析, 2021, 41(9): 2688-2695.
[6] KÜHNREICH B, WAGNER S, HABIG J C, et al. Time-multiplexed open-path TDLAS spectrometer for dynamic, sampling-free, interstitial $H_2{}^{18}O$ and $H_2{}^{16}O$ vapor detection in ice clouds[J]. Applied Physics B, 2015, 119(1): 177-187.
[7] LEWANDER M, FRIED A, WEIBRING P, et al. Fast and sensitive time-multiplexed gas sensing of multiple lines using a miniature telecom diode laser between 1 529 nm and 1 565 nm[J]. Applied Physics B, 2011, 104(3): 715-723.
[8] KOSTEREV A A, BAKHIRKIN Y A, CURL R F, et al. Quartz-enhanced photoacoustic spectroscopy [J]. Optics Letters, 2002, 27(21): 1902-1904.
[9] MA Y, HE Y, TONG Y, et al. Quartz-tuning-fork enhanced photothermal spectroscopy for ultra-high sensitive trace gas detection[J]. Optics Express, 2018, 26(24): 32103-32110.
[10] HU Y, QIAO S, HE Y, et al. Quartz-enhanced photoacoustic-photothermal spectroscopy for trace gas sensing [J]. Optics Express, 2021, 29(4): 5121-5127.
[11] MA Y, QIAO S, PATIMISCO P, et al. In-plane quartz-enhanced photoacoustic spectroscopy [J]. Applied Physics Letters, 2020, 116(6): 061101.
[12] PATIMISCO P, SAMPAOLO A, DONG L, et al. Recent advances in quartz enhanced photoacoustic sensing [J]. Applied Physics Reviews, 2018, 5(1): 011106.
[13] WANG Q, WANG Z, REN W, et al. Fiber-ring laser intracavity QEPAS gas sensor using a 7.2 kHz quartz tuning fork[J]. Sensors and Actuators B: Chemical, 2018, 268: 512-518.
[14] XU L, ZHOU S, LIU N, et al. Multigas sensing technique based on quartz crystal tuning fork-enhanced laser spectroscopy[J]. Analytical Chemistry, 2020, 92(20): 14153-14163.
[15] GIGLIO M, PATIMISCO P, SAMPAOLO A, et al. Nitrous oxide quartz-enhanced photoacoustic detection employing a broadband distributed-feedback quantum cascade laser array[J]. Applied Physics Letters, 2018, 113(17): 171101.
[16] ZHENG H, DONG L, WU H, et al. Application of acoustic micro-resonators in quartz-enhanced photoacoustic spectroscopy for trace gas analysis[J]. Chemical Physics Letters, 2018, 691: 462-472.
[17] PATIMISCO P, SAMPAOLO A, DONG L. Recent advances in quartz enhanced photoacoustic sensing [J]. Applied Physics Reviews, 2018, 5(1): 11106.
[18] GMACHL C, CAPASSO F, SIVCO D L, et al. Recent progress in quantum cascade lasers and applications[J]. Reports on Progress in Physics, 2001, 64(11): 1533-1601.
[19] SUN J, DENG H, LIU N, et al. Mid-infrared gas absorption sensor based on a broadband external cavity quantum cascade laser[J]. Review of Scientific Instruments, 2016, 87: 123101.
[20] LI J S, LIU N W, DING J, et al. Piezoelectric effect-based detector for spectroscopic application[J]. Optics and Lasers in Engineering, 2019, 115: 141-148.
[21] XU L, LIU N, ZHOU S, et al. Dual-frequency modulation quartz crystal tuning fork-enhanced laser spectroscopy[J]. Optics Express, 2020, 28(4): 5648-5657.
[22] ZHOU S, XU L, CHEN K, et al. Absorption spectroscopy gas sensor using a low-cost quartz crystal tuning fork with an ultrathin iron doped cobaltous oxide coating[J]. Sensors & Actuators B- Chemical, 2021, 326: 128951.

Dual-spectroscopy Gas Detection Technique Based on a Quartz Tuning Fork Detector

WANG Qiang, WANG Hao, XIAO Cong, LI Jinsong
(*School of Physics and Optoelectronic Engineering, Anhui University, Hefei* 230601, *China*)

Abstract: Laser spectroscopy is a powerful analytical technique based on the interaction process of light and matter (including absorption, reflection, scattering, refraction, interference, etc.), which can provide

various useful information (such as composition, concentration, velocity, flux, etc.) by analyzing the detected spectral signal and combing the related physical principles. With the continuous innovation of modern laser light sources and photodetector devices, the laser spectroscopy technique has also been developed rapidly. In terms of the three core components of the laser spectroscopy system (i.e., laser light source, absorption cell, and photodetector) and signal enhancement and noise suppression methods, various advanced laser spectroscopy techniques or detection methods have been developed. Quartz-enhanced photoacoustic spectroscopy and photothermal spectroscopy is a new and rapidly developing laser spectroscopy technique, which utilizes miniaturized quartz tuning forks as detectors with the advantages of small size, high quality factor, and low cost. Quartz-enhanced photoacoustic spectroscopy is a spectroscopic technique that measuring the aco of light and gas in a radiation-free relaxation process, which utilizes the resonance effect and piezoelectric effect of the quartz tuning fork as an acoustic detector. However, the quartz-enhanced photothermal spectroscopy technique is based on the thermoelastic effect using quartz tuning fork as a light detector. To date, quartz-based enhanced photoacoustic and photothermal spectroscopy have been successfully applied to detect many small molecules with narrow absorption spectra and several large molecules with broad, unresolved spectral absorption features. These two techniques have been widely used for developing real-time and compact trace gas sensors with high sensitivity and selectivity.

In this paper, a dual-spectroscopy detection technique based on quartz tuning forks is proposed to further improve the sensitivity of the quartz tuning fork based spectroscopic detection technique. To demonstrate this proposed gas detection technique, atmospheric water vapor (H_2O) was used for the analytic target and a dual-spectroscopy gas detection system based on two quartz tuning fork detectors (i.e. (QCTF1 and QCTF2) is developed by combing a near-infrared (NIR) diode laser emitting near 1 392 nm, the laser beam is directly coupled into an optical fiber collimator and allowing pass between the two vibrating arms of the QCTF1 detector, which is used to detect the photoacoustic signal generated from the absorption process of atmospheric water vapor. The laser beam between the two arms of the QCTF1 is then focused on the surface of the side arm of the QCTF2 detector through a CaF_2 lens, which is used to detect the photothermal signal generated in the same environmental conditions. Moreover, the wavelength tuning characteristics of the laser were measured before the experiments, and the dependence of the emission wavelength on the driving voltage of the DFB laser at a temperature of 34 ℃ was obtained to ensure that the laser emission wavelength could effectively cover the absorption line of H_2O near the optical wavelength of 1 391.67 nm. Since other gas molecules in ambient air, such as CH_4, CO, O_2 and CO_2 have not obvious absorption features near 1 391.67 nm, therefore, the spectral interference from other molecules can be effectively avoided. The resonance profile curve and the signal amplitude of the quartz tuning fork detectors are precisely measured as a function of the excitation position, and the optimal modulation frequency and excitation position are also experimentally determined, which is of great significance to improve the detection sensitivity of the proposed dual-spectroscopy detection technique. To further improving the sensitivity, the wavelength modulation technique is combined with the phase-dependent characteristics, and the effective signal enhancement of the wavelength modulated photoacoustic and photothermal spectral signals are realized by using the difference detection principle, which effectively utilizes the laser power compared with the single spectraldetection method used in the traditional detection scheme. The experimental results show that the overall Signal-to-Noise ratio (SNR) of the proposed dual-spectroscopy detection technique is 1.97 and 1.24 times higher than those of photoacoustic and photothermal spectral signal, respectively, which effectively improves the system detection sensitivity. Finally, the relationship between the photoelectric conversion efficiency of the quartz tuning fork and the incident laser power in the dual-spectroscopy detection technique is investigated. The experimental results show that the quartz tuning fork detector has a good linear response to the incident laser power with a regression coefficient $R^2=0.996$, which indicates the sensitivity can further improved by using laser sources with more high output power.

Key words: Photoacoustic spectroscopy; Photothermal spectroscopy; Quartz tuning fork detector; Dual spectroscopy techniqe; Gas detection

OCIS Codes: 140.3490; 300.1030; 300.6380

Foundation item: National Natural Science Foundation of China (Nos. 41875158, 61675005)